ACS Energy LETTERS

http://pubs.acs.org/journal/aelccp

LETTER

High Capacity for Mg^{2+} Deintercalation in Spinel Vanadium Oxide Nanocrystals

Linhua Hu, Jacob R. Jokisaari, Bob Jin Kwon, Liang Yin, Soojeong Kim, Haesun Park, Saul H. Lapidus, Robert F. Klie, Baris Key, Peter Zapol, Brian J. Ingram, John T. Vaughey, and Jordi Cabana*

Cite This: *ACS Energy Lett.* 2020, 5, 2721−2727

Read Online

ACCESS | Metrics & More | Article Recommendations | Supporting Information

ABSTRACT: **Nonaqueous Mg batteries can theoretically reach high energy density with cost-effective materials, yet no such device to date has performance competitive with Li-ion technologies. A major barrier is the need for oxide cathodes that combine high capacity and voltage. Very few oxides have shown intrinsic ability for Mg^{2+} intercalation in electrolytes with acceptably low content of H_2O. Herein, we demonstrate that nanocrystals of MgV_2O_4 can reach high capacity for Mg^{2+} deintercalation with a mechanism that preserves their spinel framework, validated through measurements with different chemical and structural sensitivity. The structural stability contrasts with other phases where reaching high capacity required distortions that introduce undesirable mechanical strain. The favorable properties of the oxide allowed cycling in a full cell with Mg metal. This work reveals new insights into the viability of multivalent intercalation in oxides, meeting a milestone toward the feasibility of high-voltage batteries with either Mg metal or Mg-ion anodes.**

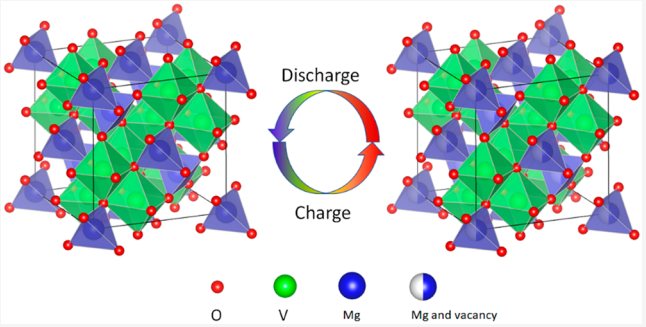

The energy density of current commercial Li-ion batteries cannot meet the stringent demands of applications in transportation and grid storage.[1,2] Despite the discovery of new cathode or anode materials and innovative engineering methods of cell design,[3−5] the capacity of the cells is pinned by the oxide cathodes, and concepts with Li metal anodes face persistent challenges to their viability.[6,7] Batteries based on low-cost Mg metal anodes are an alternative to fulfill the application requirements of high energy density because of their high volumetric capacity and the divalent nature of the transported cations, which increase the capacity per inserted ion at the cathode.[8−10] However, many challenges remain before functional devices can be assembled.[11] Chief among these challenges, the strong interaction between cations and the framework of cathode materials has so far impeded meaningful development of cathodes because of the associated low rates of Mg^{2+} diffusion.[12] While a few compounds containing soft chalcogenides can undergo stable cycling,[13,14] their low capacity and potential precludes devices with competitive energy densities.

Computational studies have predicted that a combination of voltage, capacity, and sufficient Mg^{2+} diffusion for suitable battery functionality is possible in a few oxides.[15,16] Recent experimental measurements support predictions of hopping barriers in phases with a spinel framework.[17] While evidence exists that intercalation of Mg^{2+} can be carried out in the tetrahedral sites of spinel oxides,[17−20] the capacities associated with the reactions are typically limited and the kinetics are sluggish. The situation is worse when moving from aqueous to nonaqueous electrolytes, which is required in a battery against Mg metal,[18] suggesting the existence of limitations in interfacial charge transfer that could be alleviated by nanosizing. Structural defects in spinels also play a role in the activity of the materials, but the picture remains muddled because this chemical vector offers many permutations. Antisite Mg−Mn exchange in $MgMn_2O_4$ hinders cation transport,[17,21] and excessive nonstoichiometries can promote a reversible, yet complex transformation to a layered framework.[22] In turn, poorly crystallized $MgCr_2O_4$ nanomaterials showed increased redox activity compared to highly crystalline counterparts.[19]

Vanadium oxides stand out as the chemical family showing the most promise for reversible Mg^{2+} intercalation, which has been reported for tunnel and layered polymorphs of V_2O_5.[23−25] The latter shows intrinsic ability to undergo

Received: June 1, 2020
Accepted: July 23, 2020
Published: July 23, 2020

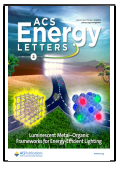

https://dx.doi.org/10.1021/acsenergylett.0c01189
ACS Energy Lett. 2020, 5, 2721−2727

intercalation at the highest reversible capacity, above 200 mAh/g, measured in an oxide in electrolytes with extremely low H_2O content. However, the high capacities demand a large distortion of the layered framework, which introduces undesirable mechanical strain that breaks down the particles.[23] Despite the attractive properties of spinels, on one hand, and vanadium oxides, on the other, no predictive[26] and very little experimental work has been devoted to MgV_2O_4 in view of its ability to act as cathode material for Mg de/intercalation. Experimental evidence from $MgCrVO_4$ indicates that V can be redox-active in spinels,[20] but the synthesis of MgV_2O_4 is elusive because of the competition from defect spinels like $Mg_3(VO_4)_2$,[27,28] which has V^{5+} and, thus, would be electrochemically inactive toward deintercalation.

Herein, we demonstrate a synthetic strategy toward MgV_2O_4 nanocrystals using a hydrothermal route. The nanocrystals show a very high intrinsic capacity toward Mg deintercalation, which is likely enabled by the lowest activation barriers to Mg hopping among spinel oxides, according to computational predictions. The extent and reversibility of the deintercalation of Mg was probed through a combination of techniques sensitive to the expected chemical, redox, and structural changes. The high activity of the MgV_2O_4 nanocrystals enabled their use in a full cell against Mg metal. This study highlights that a path exists toward Mg batteries with spinel oxides and charts a series of next steps for further advances, from the need to further understand the role of defect chemistry to an urgent call for better electrolyte systems which combine anodic stability and capability for metal plating. These advances could bring about functional nonaqueous devices with high energy density even at room temperature.

Spinel-type V_2O_4 is predicted to outperform parent variants with Mn, Co, Cr, and Ni in terms of cation mobility.[26] As depicted in Figure 1, the energy barriers for migration of Mg in

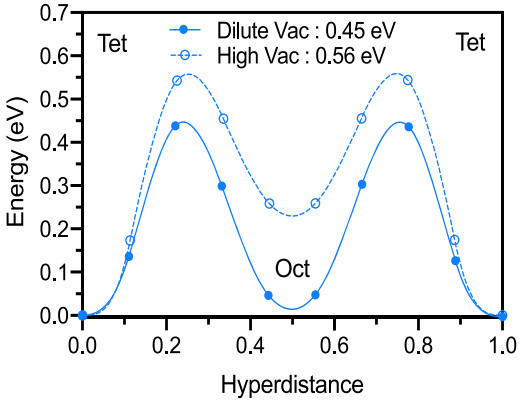

Figure 1. Minimum-energy paths for migration of Mg between the tetrahedral sites in the spinel V_2O_4 framework. The dotted and solid lines represent the migration of Mg in the high (1 Mg in empty spinel) and dilute (1 Mg vacancy in full Mg occupied spinel supercell) limits of concentration of Mg vacancies, respectively. The energy values in the legend are the migration barriers.

V_2O_4, calculated with the NEB method, are 0.45 and 0.56 eV in the dilute and high vacancy limits, respectively. To the best of our knowledge, these values are the lowest among oxide spinels calculated with the same level of exchange−correlation functional. In the dilute vacancy limit, the barrier in the V spinel is comparable to M_2O_4 with M = Mn, Co, and Ni (~0.50 eV).[26] In the high-vacancy limit, where a single Mg ion diffuses in the empty spinel, the spinel oxides based on Mn, Co, Ni, and Cr show Mg migration barriers greater than ~0.65 eV, ~0.1 eV greater than that of V_2O_4. Although the NEB calculations at the generalized gradient approximation level could underestimate the migration barrier because of difference in polaronic effects in the ground state and the transition state, our calculations imply that V spinel oxide possesses favorable cation mobility compared to previously reported transition metal spinels, motivating the evaluation of its electrochemical performance.

Elemental analysis of the as-prepared nanocrystals with ICP revealed a Mg/V ratio of 1.02/2, consistent with a MgV_2O_4 formula. Figure 2a shows the first two cycles of a half-cell at

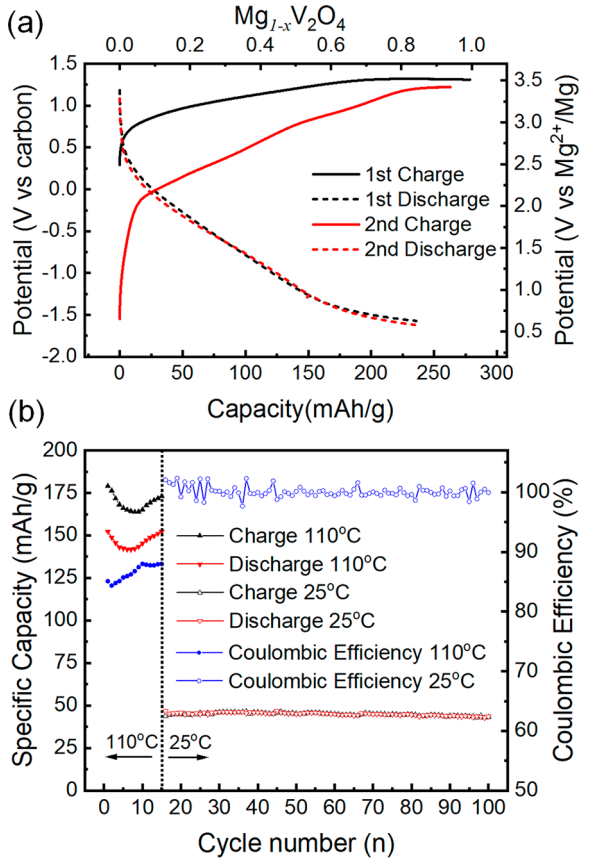

Figure 2. Electrochemical evaluation of MgV_2O_4 nanocrystals. Calculation of x is based on the theoretical capacity for full demagnesiation, 280 mAh/g. (a) Voltage profiles at 0.6−3.5 V vs Mg^{2+}/Mg^0 for electrodes in an ionic liquid Mg^{2+} electrolyte at 110 °C. (b) Cycling performance at 0.9−3.4 V vs Mg^{2+}/Mg^0 at 110 °C (15 cycles), followed by 25 °C (85 cycles).

110 °C with a MgV_2O_4 working electrode in a thermal stable ionic liquid electrolyte, $MgTFSI_2$−$PY_{14}TFSI$. The choice of temperature was based upon a combination of enhanced kinetics of the electrode and high conductivity of the electrolyte with a suitable electrochemical window.[23] Upon charge, the voltage increased from ~2.5 V to ~3.5 V vs Mg^{2+}/Mg^0, with a corresponding calculated capacity of ~280 mAh/g. The capacity corresponds to 1 mol Mg^{2+} per mole V_2O_4. The first discharge totaled ~235 mAh/g with different plateaus from 3.5 to 0.6 V vs Mg^{2+}/Mg^0, resulting in a large potential hysteresis. Subsequent charge and discharge produced similar profiles, with capacities well in excess of 200 mAh/g, and

https://dx.doi.org/10.1021/acsenergylett.0c01189
ACS Energy Lett. 2020, 5, 2721−2727

reduced hysteresis compared to the first cycle. This observation suggests that some of the barriers to the reaction are removed in the first cycle. The average potential of the observed reaction was estimated at 2.5 V vs Mg^{2+}/Mg^0, consistent with computational predictions.[15]

The stabilization of the recorded potential above 3.4 V and below 0.9 V vs Mg^{2+}/Mg^0 (~170 mAh/g) during the anodic and cathodic sweep, respectively, suggests the onset of side reactions involving the electrolyte. To avoid these side reactions, subsequent cycling was conducted under a constrained voltage window of 3.4−0.9 V vs Mg^{2+}/Mg^0. The first 15 cycles in Figure 2b were conducted at 110 °C, followed by 85 cycles at 25 °C to fully evaluate performance. At 110 °C, the capacities initially decreased up to the eighth cycle, then increased again and stabilized at 173 mAh/g after 15 cycles. The Coulombic efficiency was 84% in the first cycle, increasing in the next few cycles and final stabilizing at 88%. After the temperature was lowered to 25 °C, both charge and discharge capacity were ~45 mAh/g, with a Coulombic efficiency close to 100% in the following 85 cycles. An electrode cycled directly at 25 °C from its pristine state still presented only slightly lower capacity (Figure S1), but the hysteresis in potential was substantially higher. The decrease in hysteresis after cycling at high temperature is indicative of a conditioning of the electrode that is reminiscent of the behavior of α-V_2O_5,[23] albeit not as starkly necessary.

The as-made MgV_2O_4 sample was formed of aggregates of ~100 nm consisting of ~5 nm nanocrystals (Figure S2a,b). Atomic resolution STEM revealed their crystallinity, with a representative image along the [011] zone axis of the spinel structure shown in Figures 3a. The EDX line scan revealed a homogeneous and correlated distribution of V and Mg (Figures 3a,b and S3a) which in turn correlated with the local thickness of the aggregates. The average Mg/V ratio was 36/64 (Figure 3c), consistent with ICP analysis. The corresponding EDX map further confirmed the result of the EDX line scans (Figure S4a). The XRD (λ = 0.4127 Å) pattern of the pristine electrode could be indexed with a cubic spinel structure with space group $Fd\bar{3}m$ (Figure 4a), with the exception of a broad peak spanning 6−9°, 2θ, ascribed to the presence of carbon black. The position of the V *K*-edge X-ray absorption spectroscopy (XAS, Figure 4b) spectrum was found to be intermediate between $Li_3V_2(PO_4)_3(V^{3+})$ and VO_2 (V^{4+}). The intensity of the pre-edge peak of the pristine sample (yellow), at ~5470 eV, was also larger than that of V^{3+} (light blue) but smaller than that of V^{4+} (blue). This pre-edge represents transitions from V 1s to 3d transitions, which become intense upon loss of the centrosymmetry of the coordination environment due to p-d mixing. This intensity is known to correlate very well with the formal state of V.[29,30] Therefore, we concluded that the pristine state is above 3+. It is possible that the slight Mg excess revealed from both ICP and EDX analysis is compensated by the formation of V^{4+} defects. The presence of other defects, such as cationic and anionic vacancies, could not be discarded but could also not be evaluated because of the large XRD peaks. However, the local structure of the nanocrystals deviated from a spinel framework according to analysis of their X-ray pair distribution function (Figure S5). Aside from deviations in intensity of specific pairs (e.g., V−V and O−O in Figure S5), a peak at 1.67 Å was observed which cannot be explained by any pairs in a spinel framework. Such a short distance strongly suggests the presence of V^{5+} in tetrahedral sites,[27,28] contributing to the

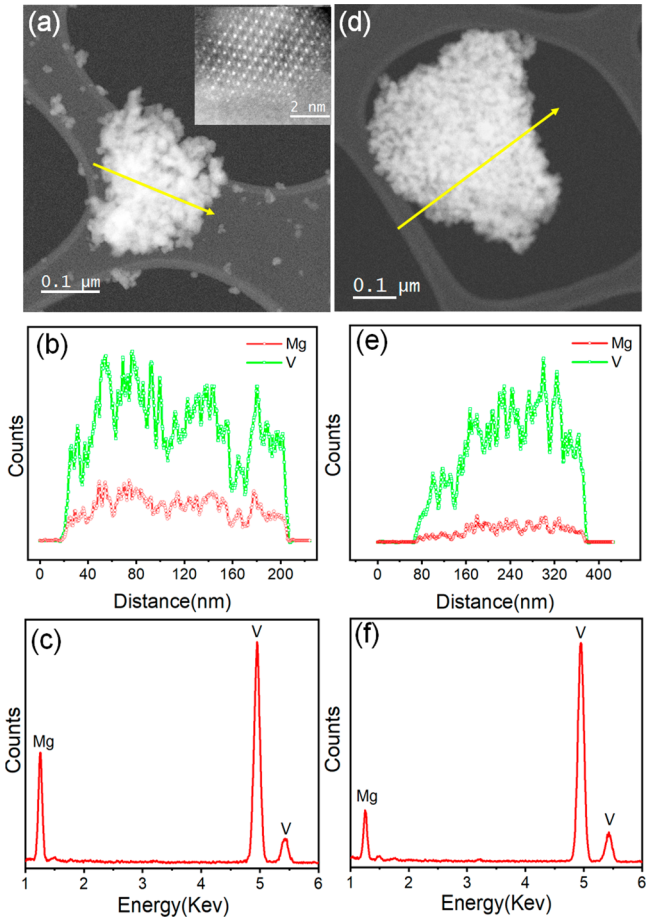

Figure 3. EDX line scan for representative pristine MgV_2O_4 nanocrystals (a−c) and charged electrode to 3.4 V vs Mg^{2+}/Mg (d−f). The yellow arrows in panels a and d indicate the direction of the line scan. Mg and V signals are represented in red and green, respectively (b and e). Average EDX spectrum with Mg and V were shown in panels c and f. An atomic-resolution STEM image of a single MgV_2O_4 particle along the [011] zone was inserted in panel a.

higher oxidation state compared to ideal MgV_2O_4. While V^{4+} and V^{5+} are difficult to distinguish by XAS,[34] XPS analysis of the pristine material suggests that ~9% V^{5+} was present (Figure S6). These observations strongly point towards a complex defect chemistry in this material, which will be the object of follow-up work.

The local homogeneity and correlation in V and Mg content were preserved after charging to 3.4 V vs Mg^{2+}/Mg^0 (Figures 3d,e and S3b). However, the average Mg/V ratio measured by EDX decreased to 19.8/80.2 across several fields of view (Figure 3f). The corresponding EDX map further confirmed the result of EDX line scan (Figure S4b). Accordingly, XRD revealed a change in the unit cell parameters from a = 8.3706(7) to 8.2754(5) Å (Table 1 and Figures 4a and S7), confirming a bulk topotactic process involving a ~3.4% volume decrease. This change in volume was significant compared to other spinel oxides,[20] indicating a much greater degree of demagnesiation. Lastly, the position of the V K-edge absorption threshold after charging (orange in Figure 4b) overlapped well with reference VO_2, confirming oxidation to 4+, but slight differences were noted in the pre-edge region, hinting at a different local V coordination environment due to

https://dx.doi.org/10.1021/acsenergylett.0c01189
ACS Energy Lett. 2020, 5, 2721−2727

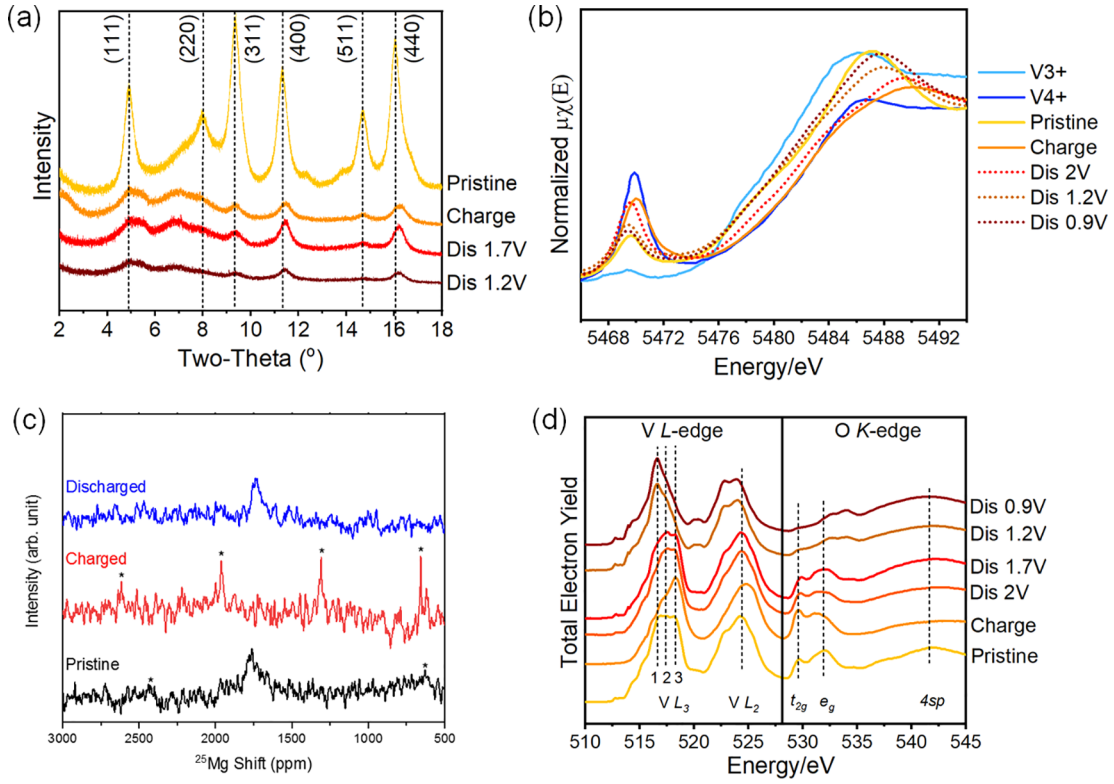

Figure 4. Multimodal analysis of MgV_2O_4 electrodes harvested from half cells at potentials vs Mg^{2+}/Mg^0 indicated in each panel. (a) High-resolution XRD results at λ = 0.4127 Å. (b) V *K*-edge XANES spectra. (c) ^{25} Mg MAS NMR spectra. (d) V $L_{2,3}$- and O *K*-edge XAS collected via TEY detection.

Table 1. Pawley Refinement Parameters for Different MgV_2O_4 Samples (Space Group $Fd\bar{3}m$) and Mg/V Ratio by EDX

samples	*a* (Å)	vol (Å^3)	R_{wp} (%)	Mg/V (EDX atom %)
pristine	8.3706(7)	586.516	3.395	36.0/64.0
charge 3.4 V	8.2754(5)	566.729	1.148	19.8/80.2
discharge 1.7 V	8.2898(7)	569.696	1.365	29.6/70.4
discharge 1.2 V	8.2931(5)	570.372	0.887	35.9/64.1
discharge 0.9 V				39/61

the different crystal structures (monoclinic vs spinel). In total, these observations support extensive deintercalation of ∼56% Mg. The deintercalation of Mg^{2+} further increased at higher potentials, with the Mg/V ratio at 14.4/85.6 after charging to 3.5 V vs Mg^{2+}/Mg^0 (Figure S8), indicating that up to ∼70% Mg could be removed from the compound, in good agreement with the capacities measured in Figure 1a.

All XRD peaks shifted back after discharge (Figure 4a). Although no new peaks appeared, there appeared to be a loss in crystallinity of the electrode (Figure S9), and the cell parameter did not fully revert to the initial value at 1.2 V (Figure 4a). Nonetheless, the reintroduction of Mg into the lattice was confirmed by ^{25}Mg solid-state nuclear magnetic resonance (NMR). A broad peak centered at ∼1760 ppm was observed in pristine MgV_2O_4, ascribed to Fermi contact between Mg^{2+}, located in tetrahedral sites in the spinel oxide, and V paramagnetic centers (Figure 4c).[31] No distinct resonances were detectable upon charging, yet the peak was restored at similar frequencies upon subsequent discharge to 1.7 V. No peaks consistent with the formation of MgO were observed (Figure S10),[32] discarding a conversion reaction. Furthermore, atomic-resolution STEM images collected after discharge revealed that the spinel structure was preserved (Figure S11). This evidence supports a topotactic mechanism of intercalation. Consistently, after discharging, the Mg/V ratio increased again (Figure S9) and the absorption threshold at the V K-edge shifted back to lower energy (Figure 4b), consistent with reduction of the transition metal. They were both close to the pristine state at 1.2 V. In total, the combined changes support a significant degree of reversibility in the reaction of Mg deintercalation. These trends continued slightly upon further discharge to 0.9 V, indicating that further reduction of V in the bulk via magnesiation was possible. When this electrode was compared to the pristine state, a slightly larger Mg/V ratio and lower threshold of the V *K*-edge were observed.

While the results presented so far support that the bulk of the electrode reversibly changed during the electrochemical reaction, measurements of V $L_{2,3}$- and O *K*-edge XAS with different probing depths also point at heterogeneity perpendicular to the supply of ions from the electrolyte. Figure 4d shows XAS collected in total electron yield (TEY) mode. Although TEY probes only 5−10 nm into a sample, this length still corresponds to whole individual nanocrystals in this material (Figures 3). Therefore, the observations correspond to the first layer of particles closest to the bulk of the electrolyte. The V $L_{2,3}$ signals below 527 eV correspond mainly to transitions from 2p to 3d states. The spectral signals between 528 and 535 eV correspond to the O pre-edge, arising from the excitation of the 1s electron to 2p states hybridized with V 3d states. Signals above 535 eV successively correspond to promotion of the O 1s electrons to O 2p-V 4s,p states, to

https://dx.doi.org/10.1021/acsenergylett.0c01189
ACS Energy Lett. 2020, 5, 2721−2727

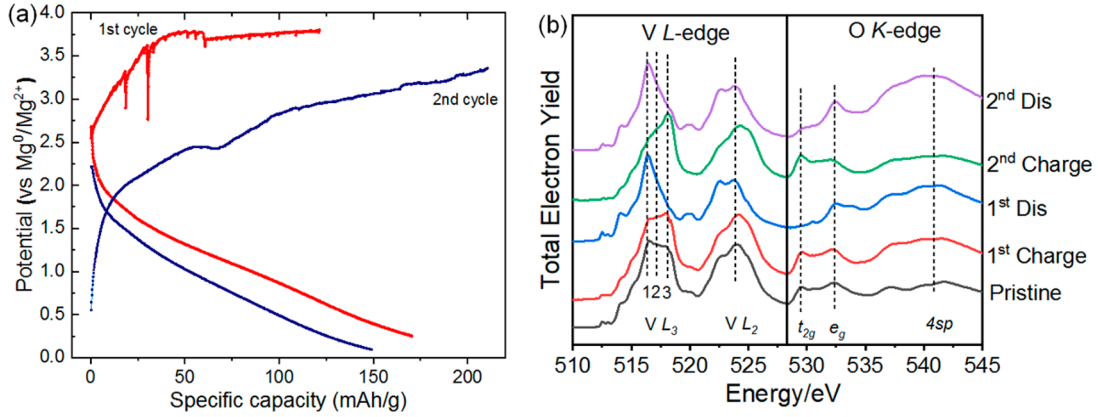

Figure 5. (a) Electrochemical properties of a Mg full cell data, Mg foil as anode, and $Mg(TPFA)_2$ as electrolyte; 85 °C, C/20, 3.8−0.25 V vs Mg^{2+}/Mg^0. (b) V $L_{2,3}$- and O *K*-edge XAS collected via TEY detection for samples harvested from these full cells.

the continuum and multiple scattering events. The pristine electrode showed V L_3 and L_2 absorption events centered at approximately 517.3 and 524.2 eV, but they were wide and complex in line shape. The O pre-edge showed two broad peaks, assigned to t_{2g} and e_g states induced by the octahedral crystal field splitting. The intensity was clearly higher for the e_g than the t_{2g} peak. Comparison with data in the literature[33] reveals that both spectra are consistent with a formal valence of V larger than 3+. The center of gravity of the V edges shifted to 518.2 and 524.9 eV upon charging, respectively. In turn, the distribution of intensity of the doublet at the O pre-edge changed, with the t_{2g} being higher than e_g. The final spectra were consistent with literature reports for VO_2.[33] The spectral changes were largely reproduced when the data was collected in total fluorescence yield (TFY), which probes 50−100 nm into the electrode (Figure S12a). Their consistence with V *K*-edge XAS indicates there was continuity between the top of the electrode and its bulk interior.

The changes were reversed after discharge. Interestingly, the center of gravity of the V L_3-edge reached approximately 516.6 eV at 0.9 V, and the intensity of the O pre-edge significantly decreased. The shape and position of V and O spectra at this potential were actually closer to those of V^{3+} oxides like V_2O_3[33] and ZnV_2O_4[34] than the those of the pristine oxide. The O pre-edge was still quite visible in the spectra collected in TFY mode (Figure S12a), despite the dampening introduced by self-absorption of fluorescent photons by the sample. However, it was still significantly shifted to higher energy than the pristine state. The decoupling of the extent of reduction observed between ensemble average measurements of the V *K*-edge and measurements of the V *L*- and O *K*-edges ∼5−10 and ∼50−100 nm into the electrode indicate the existence of gradients in the reduced states parallel to the supply of ions from the electrolyte in the coin cell format used for the experiments. This configuration favored the reaction at the top of the electrode to an extent that it reduced beyond the initial redox state.

A full cell was built with Mg metal and MgV_2O_4 nanocrystals using $Mg(TFPA)_2$ as electrolyte because of its high anodic stability.[35] In order to achieve measurable electrochemical activity, the cells had to be cycled in conditions of at least 85 °C (Figure 5a). The initial charge was sluggish, with most capacity delivered above 3.5 V. Once the electrode was discharged to 0.3 V, the kinetics improved during charge, and over 200 mAh/g could be accumulated below 3.4 and 0.2 V. The discharge profile was rather linear in both cycles, with capacities over 150 mAh/g. V $L_{2,3}$- and O *K*-edge XAS, collected with both a TEY (Figure 5b) and TFY (Figure S12b) detector, from electrodes harvested at different states of charge in the first two cycles revealed very similar reversible changes discussed for the half cells with a carbon counter electrode. The spectral changes were consistent with the cycling between V^{3+} and V^{4+}, especially in the second cycle, where the charge capacity was higher.

The electrochemical properties of sub-5 nm MgV_2O_4 nanocrystals are shown to arise from changes in Mg content that track the oxidation and reduction of V accompanied by topotactic changes that preserved the overall spinel framework. Taken together, these changes indicate that the spinel oxide is inherently capable of undergoing extensive Mg deintercalation, with capacities above 200 mAh/g at 110 °C. Some of its electroactivity was preserved even at room temperature. The large capacity and stability of the spinel framework in nonaqueous Mg electrolytes sets MgV_2O_4 apart from counterparts with Cr[19] and Mn,[18,22] even when synthesized in nanocrystalline form. The favorable Mg diffusion revealed by first-principles calculations and the moderate reaction potential of this spinel oxide enabled the use of modern Mg electrolytes compatible with metal anodes, demonstrating a clear pathway toward a functional full cell. The fact that this material operates through an initial deintercalation step could also enable the design of cells with Mg-free anodes, such as Bi.[36] For this goal to be achieved, the origins of the persistent voltage hysteresis must be understood, which demand a comprehensive set of studies of both bulk and interfacial kinetics and also the possible role of the thermodynamic reversibility and path dependence.

Aside from presenting a new candidate for Mg batteries with high energy density, this work reveals novel fundamental understanding of the control knobs of Mg intercalation in oxides, which charts a wealth of opportunities for further improvements in functionality of MgV_2O_4 electrodes. Given the good cycle life shown in half cells, failure of the full cells likely indicates that further improvements in electrolyte design are clearly critical to balance anodic stability with efficient Mg plating.[37] During discharge, reduction of the electrode domains close to the bulk electrolyte was more extensive than the bulk average, suggesting that macroscopic ionic transport was not ideal, an issue which could be circumvented with creative design of porous architectures. Encouragingly, this surface

https://dx.doi.org/10.1021/acsenergylett.0c01189
ACS Energy Lett. 2020, 5, 2721−2727

reduction also leads to the hypothesis that a broad compositional range of Mg intercalation is possible. Indeed, the materials we synthesized had a complex defect chemistry that induced the presence of V in an average state above 3+ in the pristine state. Therefore, stoichiometric MgV_2O_4 with Mg^{2+} and V^{3+} ordered in tetrahedral and octahedral sites could provide enhanced capacity for Mg deintercalation. Previous studies have also indicated that defects, especially transition metal in tetrahedral sites, must be controlled to optimize barriers to Mg diffusion.[21] A greater understanding and control of the defect chemistry of Mg−V spinels than we have today[27,28] would offer a path toward materials where both composition and structure are most optimal. The control of defects would broadly provide a general strategy to design new cathode materials to alleviate the challenge of the low Mg^{2+} mobility.

■ ASSOCIATED CONTENT

Supporting Information

The Supporting Information is available free of charge at https://pubs.acs.org/doi/10.1021/acsenergylett.0c01189.

Description of the experimental methods, as well as additional data discussed in the Letter, collected by XRD, XAS, XPS, and STEM (PDF)

■ AUTHOR INFORMATION

Corresponding Author

Jordi Cabana − *Department of Chemistry, University of Illinois at Chicago, Chicago, Illinois 60607, United States; Joint Center for Energy Storage Research, Argonne National Laboratory, Lemont, Illinois 60439, United States;* orcid.org/0000-0002-2353-5986; Email: jcabana@uic.edu

Authors

Linhua Hu − *Department of Chemistry, University of Illinois at Chicago, Chicago, Illinois 60607, United States; Joint Center for Energy Storage Research, Argonne National Laboratory, Lemont, Illinois 60439, United States;* orcid.org/0000-0002-0177-3983

Jacob R. Jokisaari − *Department of Physics, University of Illinois at Chicago, Chicago, Illinois 60607, United States*

Bob Jin Kwon − *Joint Center for Energy Storage Research and Chemical Sciences and Engineering Division, Argonne National Laboratory, Lemont, Illinois 60439, United States;* orcid.org/0000-0001-7395-0814

Liang Yin − *Joint Center for Energy Storage Research and X-ray Science Division, Advanced Photon Source, Argonne National Laboratory, Lemont, Illinois 60439, United States;* orcid.org/0000-0001-5396-782X

Soojeong Kim − *Joint Center for Energy Storage Research and X-ray Science Division, Advanced Photon Source, Argonne National Laboratory, Lemont, Illinois 60439, United States*

Haesun Park − *Joint Center for Energy Storage Research and Materials Science Division, Argonne National Laboratory, Lemont, Illinois 60439, United States;* orcid.org/0000-0001-6266-8151

Saul H. Lapidus − *Joint Center for Energy Storage Research and X-ray Science Division, Advanced Photon Source, Argonne National Laboratory, Lemont, Illinois 60439, United States;* orcid.org/0000-0002-7486-4325

Robert F. Klie − *Joint Center for Energy Storage Research, Argonne National Laboratory, Lemont, Illinois 60439, United States; Department of Physics, University of Illinois at Chicago, Chicago, Illinois 60607, United States;* orcid.org/0000-0003-4773-6667

Baris Key − *Joint Center for Energy Storage Research and Chemical Sciences and Engineering Division, Argonne National Laboratory, Lemont, Illinois 60439, United States;* orcid.org/0000-0002-1987-1629

Peter Zapol − *Joint Center for Energy Storage Research and Materials Science Division, Argonne National Laboratory, Lemont, Illinois 60439, United States;* orcid.org/0000-0003-0570-9169

Brian J. Ingram − *Joint Center for Energy Storage Research and Chemical Sciences and Engineering Division, Argonne National Laboratory, Lemont, Illinois 60439, United States*

John T. Vaughey − *Joint Center for Energy Storage Research and Chemical Sciences and Engineering Division, Argonne National Laboratory, Lemont, Illinois 60439, United States;* orcid.org/0000-0002-2556-6129

Complete contact information is available at: https://pubs.acs.org/10.1021/acsenergylett.0c01189

Notes

The authors declare no competing financial interest.

■ ACKNOWLEDGMENTS

This work was entirely supported as part of the Joint Center for Energy Storage Research (JCESR), an Energy Innovation Hub funded by the US Department of Energy (DOE), Office of Science, Basic Energy Sciences (BES), under contract DE-AC02-05CH11231. This work made use of instruments in the Electron Microcopy Service, JEOL JEM ARM200CF, Kratos AXIS-165 surface analysis system, Research Resources Center, University of Illinois at Chicago. The acquisition of this microscope was supported by an MRI-R^2 grant from the National Science Foundation (No. DMR-0959470). We acknowledge grants of computer time from ANL Laboratory Computing Resource Center (LCRC). This research used resources of the Advanced Photon Source, a U.S. Department of Energy (DOE) Office of Science User Facility operated by Argonne National Laboratory, under Contract No. DE-AC02-06CH11357.

■ REFERENCES

(1) Miao, Y.; Hynan, P.; von Jouanne, A.; Yokochi, A. Current Li-Ion Battery Technologies in Electric Vehicles and Opportunities for Advancements. *Energies* **2019**, *12*, 1074.

(2) Choi, J. W.; Aurbach, D. Promise and Reality of Post-Lithium-ion Batteries with High Energy Densities. *Nature Reviews Materials* **2016**, *1*, 16013.

(3) Evers, S.; Nazar, L. F. New Approaches for High Energy Density Lithium-Sulfur Battery Cathodes. *Acc. Chem. Res.* **2013**, *46*, 1135−1143.

(4) Bruce, P. G.; Freunberger, S. A.; Hardwick, L. J.; Tarascon, J. M. Li-O_2 and Li-S Batteries with High Energy Storage. *Nat. Mater.* **2012**, *11*, 19−29.

(5) Quinn, J. B.; Waldmann, T.; Richter, K.; Kasper, M.; Wohlfahrt-Mehrens, M. Energy Density of Cylindrical Li-Ion Cells: A Comparison of Commercial 18650 to the 21700 Cells. *J. Electrochem. Soc.* **2018**, *165*, A3284−A3291.

(6) Xu, W.; Wang, J. L.; Ding, F.; Chen, X. L.; Nasybulin, E.; Zhang, Y. H.; Zhang, J. G. Lithium Metal Anodes for Rechargeable Batteries. *Energy Environ. Sci.* **2014**, *7*, 513−537.

(7) Wood, K. N.; Noked, M.; Dasgupta, N. P. Lithium Metal Anodes: Toward an Improved Understanding of Coupled Morpho-

logical, Electrochemical, and Mechanical Behavior. *ACS Energy Lett.* **2017**, *2*, 664−672.
(8) Monti, D.; Ponrouch, A.; Araujo, R. B.; Barde, F.; Johansson, P.; Palacin, M. R. Multivalent Batteries-Prospects for High Energy Density: Ca Batteries. *Front. Chem.* **2019**, *7*, 79.
(9) Muldoon, J.; Bucur, C. B.; Gregory, T. Quest for Nonaqueous Multivalent Secondary Batteries: Magnesium and Beyond. *Chem. Rev.* **2014**, *114*, 11683−11720.
(10) Huie, M. M.; Bock, D. C.; Takeuchi, E. S.; Marschilok, A. C.; Takeuchi, K. J. Cathode Materials for Magnesium and Magnesium-ion Based Batteries. *Coord. Chem. Rev.* **2015**, *287*, 15−27.
(11) MacLaughlin, C. M. Status and Outlook for Magnesium Battery Technologies: A Conversation with Stan Whittingham and Sarbajit Banerjee. *ACS Energy Lett.* **2019**, *4*, 572−575.
(12) Canepa, P.; Sai Gautam, G.; Hannah, D. C.; Malik, R.; Liu, M.; Gallagher, K. G.; Persson, K. A.; Ceder, G. Odyssey of Multivalent Cathode Materials: Open Questions and Future Challenges. *Chem. Rev.* **2017**, *117*, 4287−4341.
(13) Aurbach, D.; Lu, Z.; Schechter, A.; Gofer, Y.; Gizbar, H.; Turgeman, R.; Cohen, Y.; Moshkovich, M.; Levi, E. Prototype Systems for Rechargeable Magnesium Batteries. *Nature* **2000**, *407*, 724−727.
(14) Sun, X. Q.; Bonnick, P.; Duffort, V.; Liu, M.; Rong, Z. Q.; Persson, K. A.; Ceder, G.; Nazar, L. F. A High Capacity Thiospinel Cathode for Mg Batteries. *Energy Environ. Sci.* **2016**, *9*, 2273−2277.
(15) Liu, M.; Rong, Z. Q.; Malik, R.; Canepa, P.; Jain, A.; Ceder, G.; Persson, K. A. Spinel Compounds as Multivalent Battery Cathodes: A Systematic Evaluation Based on Ab Initio Calculations. *Energy Environ. Sci.* **2015**, *8*, 964−974.
(16) Ling, C.; Mizuno, F. Phase Stability of Post-spinel Compound AMn_2O_4 (A = Li, Na, or Mg) and Its Application as a Rechargeable Battery Cathode. *Chem. Mater.* **2013**, *25*, 3062−3071.
(17) Bayliss, R. D.; Key, B.; Sai Gautam, G.; Canepa, P.; Kwon, B. J.; Lapidus, S. H.; Dogan, F.; Adil, A. A.; Lipton, A. S.; Baker, P. J.; Ceder, G.; Vaughey, J. T.; Cabana, J. Probing Mg Migration in Spinel Oxides. *Chem. Mater.* **2020**, *32*, 663−670.
(18) Kim, C.; Phillips, P. J.; Key, B.; Yi, T. H.; Nordlund, D.; Yu, Y. S.; Bayliss, R. D.; Han, S. D.; He, M. N.; Zhang, Z. C.; Burrell, A. K.; Klie, R. F.; Cabana, J. Direct Observation of Reversible Magnesium Ion Intercalation into a Spinel Oxide Host. *Adv. Mater.* **2015**, *27*, 3377−3384.
(19) Hu, L. H.; Johnson, I. D.; Kim, S.; Nolis, G. M.; Freeland, J. W.; Yoo, H. D.; Fister, T. T.; McCafferty, L.; Ashton, T. E.; Darr, J. A.; Cabana, J. Tailoring the Electrochemical Activity of Magnesium Chromium Oxide towards Mg Batteries through Control of Size and Crystal Structure. *Nanoscale* **2019**, *11*, 639−646.
(20) Kwon, B. J.; Lau, K. C.; Park, H.; Wu, Y. M. A.; Hawthorne, K. L.; Li, H. F.; Kim, S.; Bolotin, I. L.; Fister, T. T.; Zapol, P.; Klie, R. F.; Cabana, J.; Liao, C.; Lapidus, S. H.; Key, B.; Vaughey, J. T. Probing Electrochemical Mg-Ion Activity in $MgCr_{2-x}V_xO_4$ Spinel Oxides. *Chem. Mater.* **2020**, *32*, 1162−1171.
(21) Sai Gautam, G.; Canepa, P.; Urban, A.; Bo, S. H.; Ceder, G. Influence of Inversion on Mg Mobility and Electrochemistry in Spinels. *Chem. Mater.* **2017**, *29*, 7918−7930.
(22) Kim, C.; Adil, A. A.; Bayliss, R. D.; Kinnibrugh, T. L.; Lapidus, S. H.; Nolis, G. M.; Freeland, J. W.; Phillips, P. J.; Yi, T. H.; Yoo, H. D.; Kwon, B. J.; Yu, Y. S.; Klie, R.; Chupas, P. J.; Chapman, K. W.; Cabana, J. Multivalent Electrochemistry of Spinel $Mg_xMn_{3-x}O_4$ Nanocrystals. *Chem. Mater.* **2018**, *30*, 1496−1504.
(23) Yoo, H. D.; Jokisaari, J. R.; Yu, Y. S.; Kwon, B. J.; Hu, L. H.; Kim, S.; Han, S. D.; Lopez, M.; Lapidus, S. H.; Nolis, G. M.; Ingram, B. J.; Bolotin, I.; Ahmed, S.; Klie, R. F.; Vaughey, J. T.; Fister, T. T.; Cabana, J. Intercalation of Magnesium into a Layered Vanadium Oxide with High Capacity. *ACS Energy Lett.* **2019**, *4*, 1528−1534.
(24) Andrews, J. L.; Mukherjee, A.; Yoo, H. D.; Parija, A.; Marley, P. M.; Fakra, S.; Prendergast, D.; Cabana, J.; Klie, R. F.; Banerjee, S. Reversible Mg-Ion Insertion in a Metastable One-Dimensional Polymorph of V_2O_5. *Chem.* **2018**, *4*, 564−585.
(25) Swider-Lyons, K. E.; Love, C. T.; Rolison, D. R. Improved Lithium Capacity of Defective V_2O_5 Materials. *Solid State Ionics* **2002**, *152*, 99−104.
(26) Liu, M.; Rong, Z.; Malik, R.; Canepa, P.; Jain, A.; Ceder, G.; Persson, K. A. Spinel Compounds as Multivalent Battery Cathodes: A Systematic Evaluation Based on Ab Initio Calculations. *Energy Environ. Sci.* **2015**, *8*, 964−974.
(27) Krishnamachari, N.; Calvo, C. Refinement of Structure of $Mg_3(VO_4)_2$. *Can. J. Chem.* **1971**, *49*, 1629−1637.
(28) Wang, X. D.; Zhang, H.; Sinkler, W.; Poeppelmeier, K. R.; Marks, L. D. Reduction of Magnesium Orthovanadate $Mg_3(VO_4)_2$. *J. Alloys Compd.* **1998**, *270*, 88−94.
(29) Rees, J. A.; Wandzilak, A.; Maganas, D.; Wurster, N. I. C.; Hugenbruch, S.; Kowalska, J. K.; Pollock, C. J.; Lima, F. A.; Finkelstein, K. D.; DeBeer, S. Experimental and Theoretical Correlations Between Vanadium K-edge X-ray Absorption and K Emission Spectra. *J. Biol. Inorg. Chem.* **2016**, *21*, 793−805.
(30) Wong, J.; Lytle, F. W.; Messmer, R. P.; Maylotte, D. H. K-edge Absorption-Spectra of Selected Vanadium Compounds. *Phys. Rev. B: Condens. Matter Mater. Phys.* **1984**, *30*, 5596−5610.
(31) Lee, J.; Seymour, L. D.; Pell, A. J.; Dutton, S. E.; Grey, C. P. A Systematic Study of Mg^{25} NMR in Paramagnetic Transition Metal oxides: Applications to Mg-ion Battery Materials. *Phys. Chem. Chem. Phys.* **2017**, *19*, 613−625.
(32) Wang, H.; Senguttuvan, P.; Proffit, D. L.; Pan, B. F.; Liao, C.; Burrell, A. K.; Vaughey, J. T.; Key, B. Formation of MgO during Chemical Magnesiation of Mg-Ion Battery Materials. *ECS Electrochem. Lett.* **2015**, *4*, A90−A93.
(33) Hebert, C.; Willinger, M.; Su, D. S.; Pongratz, P.; Schattschneider, P.; Schlogl, R. Oxygen K-edge in Vanadium Oxides: Simulations and Experiments. *Eur. Phys. J. B* **2002**, *28*, 407−414.
(34) Abbate, M. The O 1s and V 2p X-ray Absorption Spectra of Vanadium oxides. *Brazilian Journal of Physics* **1994**, *24*, 785−795.
(35) Lau, K. C.; Seguin, T. J.; Carino, E. V.; Hahn, N. T.; Connell, J. G.; Ingram, B. J.; Persson, K. A.; Zavadil, K. R.; Liao, C. Widening Electrochemical Window of Mg Salt by Weakly Coordinating Perfluoroalkoxyaluminate Anion for Mg Battery Electrolyte. *J. Electrochem. Soc.* **2019**, *166*, A1510−A1519.
(36) Meng, Z.; Foix, D.; Brun, N.; Dedryvere, R.; Stievano, L.; Morcrette, M.; Berthelot, R. Alloys to Replace Mg Anodes in Efficient and Practical Mg-Ion/Sulfur Batteries. *ACS Energy Lett.* **2019**, *4*, 2040−2044.
(37) Luo, J.; He, S. J.; Liu, T. L. Tertiary $Mg/MgCl_2/AlCl_3$ Inorganic Mg^{2+} Electrolytes with Unprecedented Electrochemical Performance for Reversible Mg Deposition. *ACS Energy Lett.* **2017**, *2*, 1197−1202.

https://dx.doi.org/10.1021/acsenergylett.0c01189
ACS Energy Lett. 2020, 5, 2721−2727